Porous Membranes of Polysulfone-*graft*-poly(*tert*-butyl acrylate) and Polysulfone-*graft*-poly(acrylic acid): Morphology, pH-Gated Water Flow, Size Selectivity, and Ion Selectivity

Guojun Liu*,† and Zhihua Lu

Department of Chemistry, University of Calgary, 2500 University Drive, NW, Calgary, Alberta, Canada T2N 1N4

Scott Duncan

Defence Research Development Canada−Suffield, PO Box 4000 Station Main, Medicine Hat, Alberta, Canada T1A 8K6

Received January 6, 2004; Revised Manuscript Received March 24, 2004

ABSTRACT: Membranes were prepared from two samples of polysulfone-*graft*-poly(*tert*-butyl acrylate), PSf-*g*-P*t*BA, by immersion into water of solution films of the polymers first solvated in 1-methyl-2-pyrrolidinone (MP) and propionic acid (PA). Polysulfone-*graft*-poly(acrylic acid), PSf-*g*-PAA, membranes were obtained after soaking the PSf-*g*-P*t*BA membranes in trifluoroacetic and formic acid to hydrolyze P*t*BA. Both PSf-*g*-P*t*BA and PSf-*g*-PAA membranes had high water permeability. An electron microscopic study revealed that the membranes were porous and asymmetric. In the skin layer, the polymer formed a nodular phase consisting of fused polymer lumps surrounded by void channels. The PAA chains and presumably also the P*t*BA chains were concentrated at the lump/lump or lump/void interfaces. At a constant pressure, the water flux across PSf-*g*-PAA membranes decreased with increasing solution pH probably due to the extension of the PAA chains into the channels at high pH. The PSf-*g*-PAA membranes also showed permselectivity toward anions of lower valence and may be used to separate NaCl from Na_2SO_4, for example. A permeation test using poly(ethylene glycol) samples of different molar masses showed that membranes of a PSf-*g*-PAA sample had a size of ∼2 nm at constrictions of the nanochannels.

I. Introduction

Immersion precipitation is in wide use today for fabrication of commercial microfiltration membranes.[1] The process involves the sudden immersion of films of a concentrated polymer solution into a nonsolvent for the polymer. Currently, the technique is used to prepare membranes mainly from homopolymers including nylon, polypropylene, cellulose, and polysulfone. To modify properties such as to introduce hydrophilicity or stimuli response, one normally grafts another functional polymer on to the pore walls of a premade homopolymer membrane.[2] Unfortunately, such treatment also changes the membrane pore size and pore size distribution and thus reduces the permeation flux. One way to overcome this shortcoming is to prepare porous membranes from premade graft or block copolymers, where one part of the copolymer renders the desired mechanical property and the other part renders functions such as pore surface hydrophilicity. Reports of such work have emerged only recently mainly from Kang and coworkers,[3] who have studied membranes comprised of poly(vinylidene fluoride)-based graft copolymers. In this paper, we report the preparation of membranes from two polysulfone-*graft*-poly(*tert*-butyl acrylate) or PSf-*g*-PtBA samples (Chart 1). Also reported in this paper is the preparation of polysulfone-*graft*-poly(acrylic acid) or PSf-*g*-PAA membranes from the hydrolysis of the PSf-*g*-P*t*BA membranes. This is then followed by a discussion of the morphology, water transport, and ion transport properties as well as the size selectivity of the PSf-*g*-PAA membranes. PSf was targeted as the backbone of the graft copolymers because it possesses the desired mechanical, thermal, and chemical properties and is used widely as a commercial membrane material.[1] P*t*BA was chosen for its ready hydrolysis to yield the hydrophilic functional PAA chains.

II. Experimental Section

Materials. Trifluoroacetic acid (99%), formic acid (96%), and 1-methyl-2-pyrrolidinone (99%) were purchased from Aldrich. Propionic acid (99%) and barium chloride dihydrate (99%) were obtained from BDH Laboratory Supplies. Sodium sulfate (99.0%), sodium chloride (99.0%), sulfuric acid (95.0−98.0%), and hydrochloric acid (36.5−38.0%) were products of Merck KGaA. Poly(ethylene glycol) or PEG standards (M_w = 3070 g/mol, M_w/M_n = 1.06 and M_w = 960 g/mol, M_w/M_n = 1.07) were purchased from Scientific Polymer Products, Inc. Sodium hydroxide (98%) and potassium ferricyanide (analytical reagent) were purchased from Matheson Coleman and Bell Manufacturing Chemists, respectively.

The two PSF-*g*-P*t*BA samples used in this study were prepared by grafting bromine-terminated P*t*BA or P*t*BA-Br onto lithiated PSf following procedures described before.[4] The weight-average molar masses M_w of PSf and P*t*BA-Br were determined by light scattering (LS), and their polydispersity M_w/M_n were determined by size exclusion chromatography (SEC) based on poly(methyl methacrylate) standards. Table 1 summarizes the characteristics of the polymers with n_w and n_n denoting the weight- and number-average repeat units for the polymers. For the higher accuracy of n_w than n_n, the graft copolymers will be denoted as PSF-*g*-P*t*BA_{90} and PSF-*g*-P*t*BA_{340} with the numbers in the subscripts defining n_w for the P*t*BA branches.

The graft copolymers were carefully characterized by ^{1}H NMR to yield the number-average number n_b of P*t*BA branches per PSf chain. With $n_b \approx 0.85$, the graft copolymers consist of a mixture of PSf-*g*-P*t*BA and PSf. The characteristics of the graft copolymers are given in Table 2.

† Current address: Department of Chemistry, Queen's University, Kingston, Ontario, Canada K7L 3N6.

10.1021/ma049954q CCC: $27.50
Published on Web 05/08/2004

Chart 1

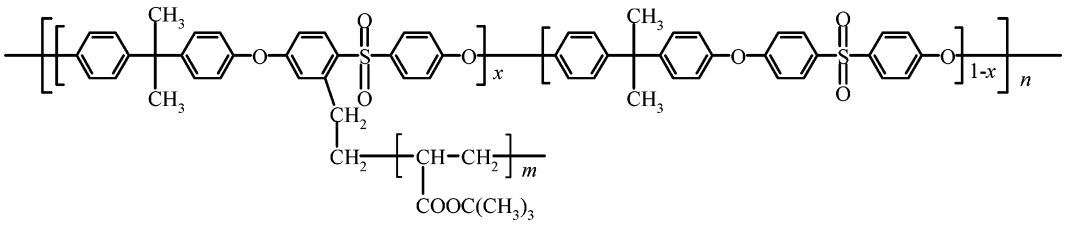

Table 1. Characteristics of P*t*BA and PSf

sample	LS $10^{-4}M_w$ (g/mol)	n_w	SEC M_w/M_n	n_n
P*t*BA$_{90}$-Br	1.11	90	1.26	71
P*t*BA$_{340}$-Br	4.3	340	1.40	242
PSf	6.8	150	1.67	90

Table 2. Characteristics of the PSf-*g*-P*t*BA Samples

sample	P*t*BA (vol %)	n_b	SEC M_w (g/mol)	SEC M_w/M_n
PSf-*g*-P*t*BA$_{90}$	19.2	0.88	124 000	1.96
PSf-*g*-P*t*BA$_{340}$	44	0.83	209 000	2.49

PSf-*g*-P*t*BA Membrane Preparation. PSF-*g*-P*t*BA solution films were prepared on microscope slides by dipping the slides into a 15.0 wt % PSf-*g*-P*t*BA solution in 1-methyl-2-pyrrolidinone (MP) and propionic acid (PA) (wt/wt = 70/30). The subsequent immersion of the solution films into a water bath yielded the desired membranes. An example procedure involved first dissolving 1.50 g of PSf-*g*-P*t*BA$_{90}$ in 8.5 g of MP/PA in a cell ($1.8 \times 2.7 \times 9.7$ cm^3) resembling the shape of a cuvette used for UV−vis absorbance measurement. To minimize solvent evaporation during polymer dissolution by magnetic stirring, the top opening of the cell was sealed with two layers of Teflon tape and two layers of paraffin film. After air bubble removal from the solution by centrifugation at 1100*g* for 3 min, a glass slide ($0.1 \times 2.5 \times 5.5$ cm^3) was immersed into the solution. To minimize solvent evaporation, the cell was immediately sealed by stretching the thumb portion cut from a powder-free rubber glove over the opening. This permitted the glass slide to be manipulated using a pair of tweezers by gripping it through the thin layer of rubber. The cell was inclined in order to fully immerse the surface of the glass plate. After several minutes, the cell was returned to the vertical position, and the glass plate was removed from the solution phase. The plate was held in a vertical orientation above the solution for 30 s to allow the excess solution to drain from the surface and then immersed in 100 mL of distilled water. Several minutes after immersion the membrane detached from the glass plate. It was left free-floating for 3 h. Following this, the membrane was transferred into a new bath containing 1 L of water for storage. Only the center part of the membrane (2.0×2.0 cm^2) was used in the investigations to be discussed.

PSf-*g*-PAA and PSf-*g*-PSA Membranes. PSf-*g*-P*t*BA membranes were taken out of water and their surfaces dried with filter paper. They were further dried under ambient conditions for 24 h before immersion in 5.0 mL of trifluoroacetic and formic acid (v/v = 10/90) for 24 h to hydrolyze the *tert*-butyl groups of P*t*BA. After this, the membranes were soaked in distilled water for 3 h. Before a permeability test was conducted, a membrane was first soaked in 20 mL of a NaOH solution at pH = 10.0 for 6 h. Then it was immersed in distilled water (changed several times) for 3 h. This was followed by soaking in HCl solution at pH = 2.0 for 3 h and a further immersion in distilled water for 3 h. These steps were repeated a second time and were performed to anneal the membranes for reproducible permeability data. Membranes in the poly(sodium acrylate) or PSA form or PSf-*g*-PSA membranes were obtained by soaking the PSf-*g*-PAA membranes in 20 mL of a NaOH solution at pH = 10.0 for 6 h and in distilled water changed several times for 3 h.

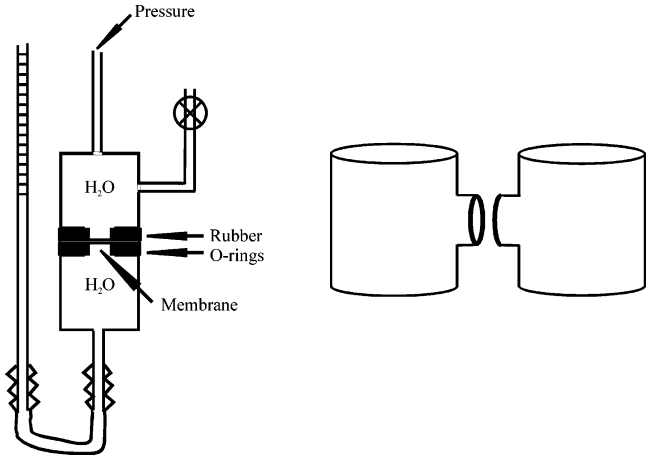

Figure 1. Cells used for testing water (left, a) and salt (right, b) permeation.

Scanning Electron Microscopy (SEM). Surface and cross-sectional images of the PSf-*g*-P*t*BA and PSf-*g*-PAA membranes were taken using a FEI XL310 ESEM scanning electron microscope. To obtain the cross-sectional images, samples were fractured after soaking in liquid nitrogen. The fractured membrane was cut ∼1 mm from the fractured surface to yield a thin strip. The strip was then mounted with the fractured surface facing up on a double-sided adhesive carbon tape (Electron Miscroscopy Sciences), which had been glued on to a stainless steel sample support. To obtain an image of the surface of the membrane, a small piece was mounted horizontally on carbon adhesive tape. Before viewing, the samples were coated with a 6 nm thick platinum−gold layer using a Hummer I sputter coater.

Transmission Electron Microscopy (TEM). A PSf-*g*-PAA membrane was sandwiched between two 1.5 mm thick polystyrene plates, which had been preheated to 110 °C. The PS plates were lightly pressed to promote adhesion. The fused plates were microtomed using an Ultracut-E Reichert-Jung instrument to yield thin sections with thickness ∼50 nm. The sections were picked up by Formvar-coated copper grids and stained by several drops of a 3.0 wt % uranium acetate solution in ethanol/water (v/v = 1/9) for 15 min. The excess solution was sucked away with a filter paper placed at the bottom side of the grid. The thin sections were then rinsed with water droplets thrice before viewing under a Hitachi-700 electron microscope operated at an accelerated voltage of 75 kV.

Permeation Cells. The PSf-*g*-PAA membranes were tested for their water, PEG, and salt permeability. Water permeability was tested using a stainless steel cell with design shown in Figure 1a. The permeation area of the membrane was 2.01 cm^2. The design of the cell used for testing the permeability of PEG and salts is shown in Figure 1b. The volume of each half cell in this case is ∼16 mL, and the permeation area of the membrane is 0.985 cm^2.

Water Permeability Test. Pressurized nitrogen was used to exert pressure on a permeating aqueous solution or water. The pressure was controlled using a two-stage regulator. The pH value of distilled water was adjusted by adding 1.0 M NaOH or HCl solution. To obtain the steady-state flux of an aqueous solution at a given pH, the permeation cell was rinsed

with the solution thrice, and 10 mL of the solution was then pushed through the membrane. The liquid on both the permeate and feed sides was discarded and replaced with a fresh solution. The readings at 1.00 atm were obtained in triplets or quadruplets only after another 10 mL of the fresh solution was pushed through the membrane. The variation in water flux as a function of pH in the aqueous phase was monitored under two sets of conditions. In the first case, the experiment was performed without adding NaCl, except the addition of NaOH or HCl to adjust the solution pH. In the second case, the experiment was done at a constant NaCl concentration of 0.050 M.

To examine the response of water flux to a sudden pH change, only one reading was taken at a particular time. The time required to obtain one flux reading ranged typically between 2 and 3 s and was always <6 s. The PSf-*g*-PAA and PSf-*g*-PSA membranes were prepared following procedures described above. Prior to permeability tests on PSf-*g*-PSA membranes with solutions at pH = 2.0 or PSf-*g*-PAA membranes with solutions at pH = 8.0, 10 mL of distilled water was pushed through the membranes to purge and clean them.

PEG Permeation Experiment. To prevent damage, a PSf-*g*-PAA_{90} membrane was sandwiched by two paraffin rings with an opening of 0.985 cm^2 in the center. The sandwiched membrane was then inserted at the joint between the two half-cells designed as shown in Figure 1b. The two half-cells were held together with several elastic bands. To test the cutoff molar mass of the membrane, 13.00 mL of an aqueous solution of the two PEG samples with M_w = 3070 and 960 g/mol each at 10 ppm was added to one half-cell and dialyzed against 13.00 mL of distilled water. The liquid in the half-cells was constantly stirred, and aliquots at either 0.40 or 0.20 mL were taken from both sides at predesignated times. Liquid was taken from both sides to minimize solution flow driven by hydrostatic pressure difference. The sample from the permeate side was heated at 80 °C for 12 h to evaporate water. Tetrahydrofuran (THF, 0.20 mL) was then added to dissolve the polymer for sample analysis by SEC using a Waters HT-4 column at a flow rate of 1.00 mL/min.

Samples for PEG-960 dialysis kinetic study were prepared similarly, where PEG-960 denotes PEG with the weight-average molar mass of 960 g/mol. The pH on the feed and permeate side was made the same by adding either 1.0 M HCl or 1.0 M NaOH solution. The concentration of PEG on the permeate side was obtained from the SEC peak height against a calibration curve.

Salt Permeation. Salt permeation experiments were performed using the cell design shown in Figure 1b. The initial salt concentration on the feed side was 1.00×10^{-3}, 0.50×10^{-3}, 0.50×10^{-3}, and 0.33×10^{-3} M for NaCl, Na_2SO_4, $BaCl_2$, and $K_3[Fe(CN)_6]$, respectively. The concentration increase of NaCl, Na_2SO_4, and $BaCl_2$ on the permeate side was followed by a conductometer. The volume of the feed solution was 16.00 mL, and that of water on the permeate side was 14.00 mL. The liquid volume on the feed and permeate side differed due to the volume occupied by the conductivity probe. The $K_3[Fe(CN)_6]$ concentration increase on the permeate side was followed by absorbance change at 418 nm, and the solution volume used was 15.0 mL.

III. Results and Discussion

Preparation of PSf-*g*-P*t*BA Membranes. Despite many reports on the preparation of microfiltration membranes from PSf[1] and its derivatives[5] by the immersion precipitation method, we did not find literature on membrane preparation from preformed PSf-based graft copolymers. Preparation of microfiltration PSf membranes by the immersion precipitation method normally involved the immersion into water of solution films of PSf in MP, *N*,*N*-dimethylformamide (DMF), or dimethyl sulfone. As a starting point, we tried to prepare PSf-*g*-P*t*BA membranes under similar conditions by dissolving the PSf-*g*-P*t*BA copolymers in MP or DMF and then the immersion of the solution films in water. Unfortunately, we failed to detect water permeability in the resultant membranes. Our water-permeable membranes were prepared by immersing into water solution films cast from PSf-*g*-P*t*BA_{90} or PSf-*g*-P*t*BA_{340} solvated in MP/PA.

Table 3. Cloudy Points of Various Polymers

sample	solvent	water (wt %)
PSf	MP	8.0
PSf-*g*-P*t*BA_{90}	MP	8.3
PSf-*g*-P*t*BA_{340}	MP	8.6
PSf	MP/PA (v/v = 7/3)	2.9
PSf-*g*-P*t*BA_{90}	MP/PA (v/v = 7/3)	3.5
PSf-*g*-P*t*BA_{340}	MP/PA (v/v = 7/3)	3.9

Membranes prepared by the immersion precipitation method normally have an asymmetric structure with the smallest pores located in the skin layer, which acts to limit the rate of reagent transport.[1] The pore structure is interconnected and transports liquid only if the polymer phase separates immediately, e.g., in less than ~1 s, after the immersion of a solution film into a nonsolvent. This has been traditionally achieved by using high-affinity solvent and nonsolvent pairs to facilitate their fast mixing in the skin layer during membrane formation. We failed to prepare water-permeable PSf-*g*-P*t*BA membranes under identical conditions used for PSf membrane preparation probably because the phase separation of PSf-*g*-P*t*BA from MP/water was slower than that of PSf. Notably, more water was required to induce PSf-*g*-P*t*BA phase separation as shown by data of Table 3. At an initial polymer concentration of 10.0 mg/mL in MP, we, for example, determined the amount of water required to introduce visual cloudiness for PSf, PSf-*g*-P*t*BA_{90}, and PSf-*g*-P*t*BA_{340} to be 8.0, 8.3, and 8.6 wt %, respectively.

PA is a good solvent for P*t*BA and a nonsolvent for PSf and has high affinity for water. Its addition to a casting solution consisting of PSf in MP has been reported to enhance pore formation of PSf membranes and thus increased membrane water permeability.[6] The explanation offered by Han was that the addition of PA decreased the amount of water required to cause PSf phase separation and thus enhanced the rate of polymer phase separation. The same mechanism must have operated here, as data of Table 3 clearly show that the addition of PA decreased the amount of water required to cause PSf and PSf-*g*-P*t*BA to phase separate. For the PSf sample, the addition of 30 wt % of PA to MP lowered the cloudy point from 8.9 to 2.9 wt % of water. The same decreasing trend was seen for the PSf-*g*-P*t*BA samples.

The membranes used in this study were prepared from casting into water 15.0 wt % of PSf-*g*-P*t*BA_{90} or PSf-*g*-P*t*BA_{340} in MP/PA. The resultant dry membranes were 90 ± 5 μm thick.

PSf-*g*-PAA Membranes. PSf-*g*-PAA membranes were obtained after the hydrolysis of the PSf-*g*-P*t*BA membranes in trifluoroacetic and formic acid. The quantitative hydrolysis of the P*t*BA groups was established by performing ^{1}H NMR analysis of the hydrolyzed membranes after their dissolution in deuterated DMF. After hydrolysis, the PSf-*g*-PAA_{90} membranes had a dry thickness of 80 ± 5 μm and were robust under all testing conditions. The PSf-*g*-PAA_{340} membranes swelled substantially in water. Because of swelling, the PSf-*g*-PAA_{340} membranes became so soft in water that two of such membranes easily fused together. The membranes also wrinkled readily in basic water.

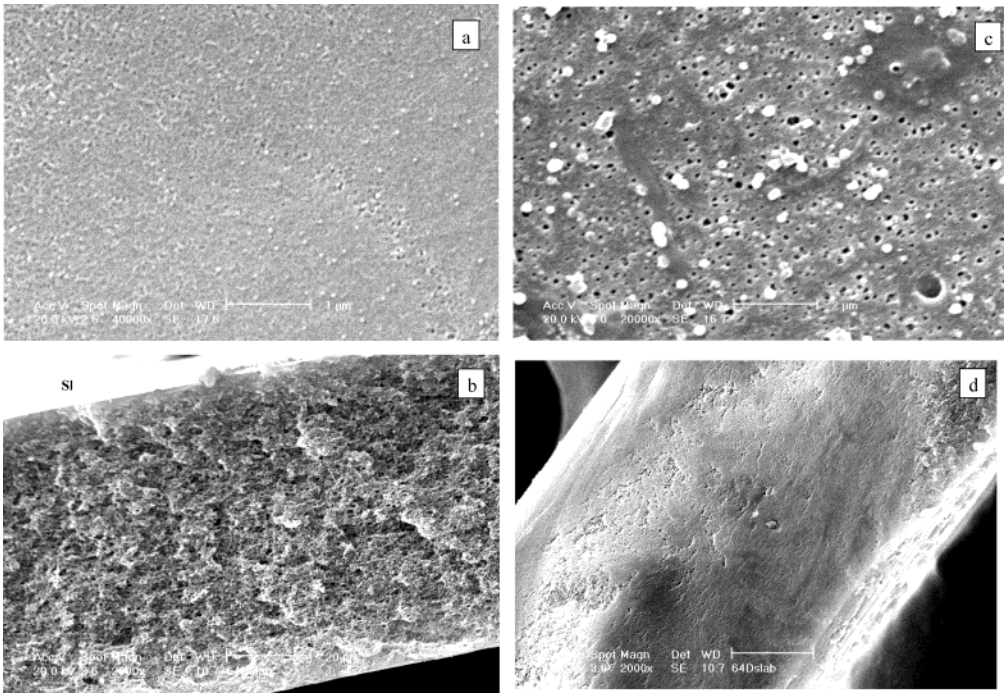

Figure 2. SEM images of the top surface (a), the cross section (b), and the bottom surface of a PSf-*g*-P*t*BA$_{90}$ membrane. Also shown is a cross-sectional SEM image of a PSf-*g*-PAA$_{90}$ membrane (d).

Morphologies of the PSf-*g*-P*t*BA$_{90}$ and PSf-*g*-PAA$_{90}$ Membranes. Figure 2a shows a SEM image of the surface of the skin layer of a PSf-*g*-P*t*BA$_{90}$ membrane. There are some small pores on the surface of the skin layer. Also obvious on the surface, especially at the top left corner of the image, is an undulating wavy pattern with the dark domains corresponding to the valleys or pores and the light regions corresponding to the granular or nodular protrusions. Figure 2b shows an image of the whole cross section. The membrane is more dense at the surfaces and more porous in the center. At the bottom surface (Figure 2c), the pores are smaller than those in the center but larger than those in the skin layer.

Figure 2d shows a cross-sectional image of a PSf-*g*-PAA$_{90}$ membrane. A comparison between parts b and d of Figure 2 suggests that the hydrolysis resulted in the collapse of the relatively large pores and compaction of the membranes. An examination of an image at a higher magnification indicated that the smaller pores were, however, not affected by hydrolysis.

Figure 3a shows a TEM image of a thin section of the skin layer of a PSf-*g*-PAA$_{90}$ membrane. The contrast in Figure 3a derives from fluctuations in the density of the copolymer. The fact that the polymer forms an interconnected "dark" nodular phase is unambiguously verified here. Surrounding the polymer granules are the "light" cracks or channels, which would have been difficult to see by SEM. The distribution of the PAA and PSf chains can be discerned from Figure 4b. The PAA chains should look darker here, as they were stained by U(Ac)$_2$. The PAA chains are concentrated at the granule/crack and granule/granule interfaces. More convincing evidence for this conclusion is presented in Figure 4c, where a TEM image of a thin section of the skin layer of a PSf-*g*-PAA$_{340}$ membrane is shown. The PAA chains are more readily discerned here due to their higher concentration.

In summary, the following model emerges from the TEM and SEM study. First, the membranes are asymmetric with the smallest pores or cracks in the skin layer. Farther away from the skin layer, the pores become larger and are better defined in shape. The pore size decreases again in the bottom layer but is substantially larger than those in the skin layer. Second, the polymer forms a nodular phase in the skin layer but a homogeneous continuous phase in the bottom layer. Third, the PAA chains in the skin layer are concentrated at the granule/crack and granule/granule interfaces.

Water Flux Variation as a Function of Pressure. Figure 4 shows how the flux f of distilled water varies as a function of pressure p for the PSf-*g*-P*t*BA$_{90}$ and PSf-*g*-PAA$_{90}$ membranes. As p increases, f increases as expected. There are, however, two surprising features. First, f did not increase linearly with p for the membranes. Rather, the f vs p curves exhibited an upward curvature. Second, the f values of the PSf-*g*-PAA$_{90}$ membrane were lower than those of the PSf-*g*-P*t*BA$_{90}$ membrane at all examined pressures.

The nonlinear increase of f with p normally suggests membrane structural instability.[2b] Our morphological study showed that water flow along the cracks in the internodular space in the skin layer was rate-limiting. As pressure increased, the pressure could have exerted sufficient force on the nodules and forced them to open up more, thus making f to increase more than linearly with p. The other possibility is that higher pressures are required to wet the smaller channels and thus to push water through them. The f values increased more than linearly with p because the number of transporting channels increased in the membrane with increasing p.

To check whether the higher f values for the PSf-*g*-P*t*BA$_{90}$ membrane were of statistical significance, we measured the permeability of pH = 2.0 water across three PSf-*g*-P*t*BA$_{90}$ and three PSf-*g*-PAA$_{90}$ membranes. The average f are $(8.40 \pm 0.18) \times 10^{-3}$ and $(7.96 \pm 0.28) \times 10^{-3}$ mL/(s cm^2) for the PSf-*g*-P*t*BA$_{90}$ and PSf-*g*-PAA$_{90}$ membranes, respectively, with the numbers after the $\pm$ signs denoting the standard deviations. These values suggest that the difference was real. Such a difference

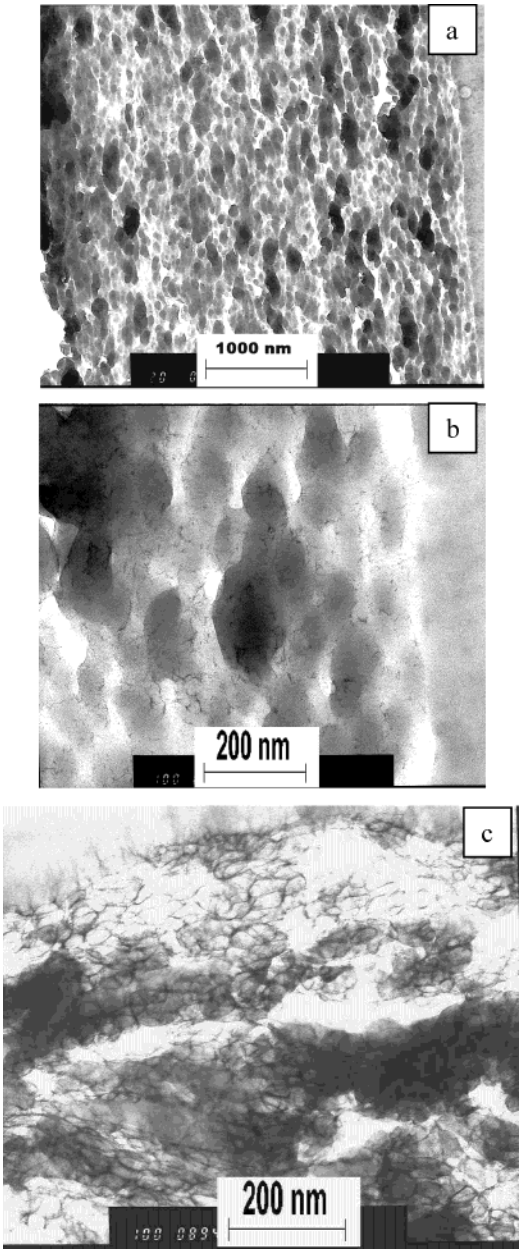

Figure 3. TEM images of thin sections of PSf-*g*-PAA membranes. Images a and b were obtained for a PSf-*g*-PAA_{90} membrane, and image c was for a PSf-*g*-PAA_{340} membrane.

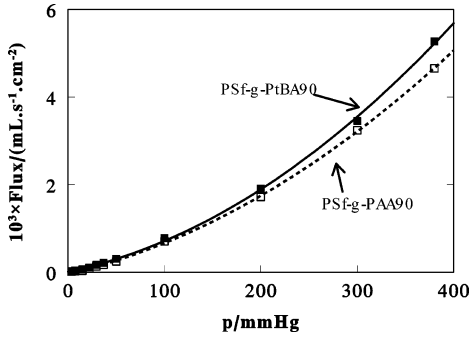

Figure 4. Variation in permeation rate of distilled water as a function of applied pressure *p* for a PSf-*g*-P*t*BA_{90} (■) and a PSf-*g*-PAA_{90} (□) membrane.

has also been noted for many other membranes that were not included in the statistical analysis. The flux of the PSf-*g*-PAA_{90} membranes remained lower than

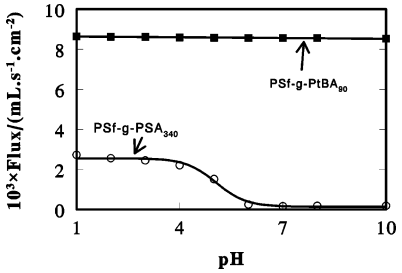

Figure 5. Variation in water flux *f* as a function of pH for a PSf-*g*-P*t*BA_{90} (■) and a PSf-*g*-PSA_{340} (○) membrane at an applied pressure of 1.00 atm.

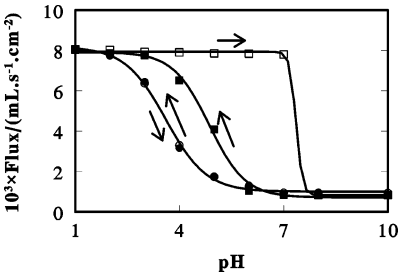

Figure 6. Variation in water flux *f* as a function of pH for a PSf-*g*-PAA_{90} membrane in the absence (□, ■) and presence (○, ●) of 0.050 M NaCl, respectively. The empty symbols represent data obtained by increasing pH from 1.0 to 10.0, and the solid symbols represent data obtained by decreasing pH from 10.0 to 1.0.

that of the PSf-*g*-P*t*BA_{90} membranes probably for two reasons. First, the PSf-*g*-P*t*BA_{90} membranes are more porous as confirmed by our morphological study. Second, the P*t*BA chains, unlike the PAA chains, did not extend into the cracks to impede water flow.

Water Flux Variation as a Function of pH. Figures 5 and 6 show how *f* for the PSf-*g*-P*t*BA_{90}, PSf-*g*-PAA_{90}, and PSf-*g*-PSA_{340} membranes varies with pH and the concentration of NaCl at $p = 1.00$ atm. The *f* values of the PSf-*g*-P*t*BA_{90} membrane changed significantly with neither pH nor the concentration of NaCl because the membrane contained no pH-responsive polyelectrolyte chains. This is in contrast to the *f* variation trends of the PSf-*g*-PAA_{90} or PSf-*g*-PSA_{340} membranes. For these membranes, *f* was substantially larger in the PSf-*g*-PAA form (lower pH) than in the PSf-*g*-PSA form (higher pH). The more surprising result was that *f* in Figure 6 at a given solution pH between 5.0 and 7.0 differed depending on the history of the membrane. Starting from PSf-*g*-PAA_{90} and increasing solution pH gradually, we found that *f* remained essentially constant until pH = 7.0 and then dropped abruptly. Starting from PSf-*g*-PSA_{90} and decreasing solution pH, the *f* values remained low and increased quickly only after pH = 6.0. In the presence of 0.050 M NaCl, the *f* value at a given solution pH was unique and independent of the initial state of the membrane.

The phenomenon of pH-gated water flow for membranes containing grafted PAA chains has been observed by many groups[2,3] and has been explained by invoking conformational changes of the grafted PAA chains with pH. The explanation applies equally well here. In our case, the PAA chains extend into the cracks between the PSf nodules in the skin layer. As pH increases, the acrylic acid groups of the PAA chains get progressively deprotonated, and thus the PAA chains assume more extended conformations due to electrostatic repulsion between intrachain segments. The more

extend PSA chains impose increased hydrostatic resistance and slow down water flow.

The *f* ratios at pH = 1.0 and pH = 10.0 are 9.6 and 14.6 for the PSf-*g*-PAA_{90} and PSf-*g*-PAA_{340} membranes, respectively. The *f* ratio at the two pH's is higher for the PSf-*g*-PAA_{340} than for the PSf-*g*-PAA_{90} membrane probably for the more efficient blocking of the transporting channels or cracks by the PSA_{340} chains at pH = 10.0. The blocking had been more efficient, first, for the smaller cracks found in the PSf-*g*-PAA_{340} membrane as evidenced by the considerably lower *f* values at low pH's for this membrane. Then, the grafted PSA_{340} chains are longer, and these make the fraction of cross-section area accessible by the PSA_{340} chains in the cracks at high pH larger than that in the PSf-*g*-PSA_{90} membrane. An enhancement in the pH-gating effect by increasing PSA graft density has been observed before. Liu et al.[7] have, for example, prepared thin films containing uniform cylindrical channels of a diameter of ~20 nm from a diblock copolymer. Grafted onto the wall of the channels was a PSA block with 380 units. Since the PSA grafting density was high and the PSA chains were long, Liu et al. observed a ~1000-fold variation in *f* by increasing the pH from 3 to 10.

The variation of *f* at a given solution pH with the history of the membrane surprised us initially. As mentioned before, *f* varied because of the conformation change of the PAA chains with increasing degree *x* of AA group deprotonation. In the membrane, *x* is related to the acid dissociation constant K_a and pH by

$$\log \frac{x}{1-x} = \log K_a + \mathrm{pH} \qquad (1)$$

Since K_a is a constant, the fact that *f* differed at a given aqueous solution pH suggests that pH inside the membrane was not the same as that in the aqueous phase.

The pH inside a PSf-*g*-PAA or PSf-*g*-PSA membrane may differ from or be lower than that in the aqueous phase at low salt concentrations for the fact that the carboxyl-group-containing membrane rejected anions but sorbed cations such as H^+ and Na^+ selectively.[1] The pH inside a membrane may further vary at a given solution pH depending on the history of the membrane because membranes from different initial states contained different types of ions or the same type of ions at different concentrations. For a PSf-*g*-PAA membrane in equilibrium with water at pH = 5.0, for example, the cations found in the membrane are essentially H^+. On the other hand, the cations can be either H^+ or Na^+ in a PSf-*g*-PSA membrane in equilibrium with water at pH = 5.0. Thus, the condition for electric neutrality in the membrane in the former case is

$$[H^+] = [COO^-] + [Cl^-] + [OH^-] \qquad (2)$$

It becomes

$$[H^+] + [Na^+] = [COO^-] + [Cl^-] + [OH^-] \qquad (3)$$

in the latter. In the presence of Na^+, the appetite of the membrane for cations was met mostly by the sorption of Na^+. Therefore, the pH inside the membrane should have been closer to that in the aqueous phase than in the former case, and a lower external pH was required to induce the *f* transition as seen in Figure 6 for the curve obtained by decreasing pH from 10.0 to 1.0.

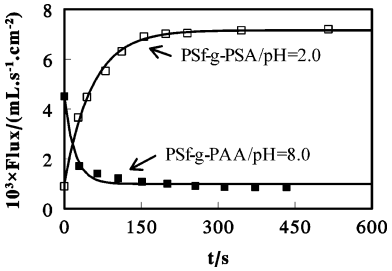

Figure 7. Variation in the water permeation flux of a PSf-*g*-PSA_{90} (□) or PSf-*g*-PAA_{90} (■) membrane as a function of time after water at pH = 2.0 and pH = 8.0 was introduced at 1.00 atm, respectively.

Increasing the NaCl concentration to 0.050 M would have increased Na^+ uptake further at the cost of H^+ uptake. This made the pH in the aqueous phase approximately equal to or higher than that in the membrane phase. In this case, the *f* data became independent of the history of the membrane as seen for data of Figure 6. The decrease in the pH inside the membrane by increasing NaCl concentration has exhibited itself by showing an additional shift in the *f* curve to the lower pH side as witnessed in Figure 6. In the presence of NaCl, the midpoint of the *f* transition occurred at pH ≈ 3.8, which is lower than the pK_a value of 4.75 reported for PAA in the literature[8] and suggests that the pH inside the membrane was probably higher than that in the aqueous phase.

Water Flux Variation with Sudden pH Changes. The pH-gated water flow, with the gating pH tunable by varying the ionic strength of the aqueous phase and the membrane history, may have practical applications in controlled drug or fertilizer release. For these applications, it is important to know how fast the water flux changes in response to a sudden jump or dip in pH. Figure 7 shows such data. After the introduction of pH = 2.0 water, the flux *f* across a PSf-*g*-PSA membrane increased exponentially with time *t* following

$$f = f_\infty - a \exp(-t/\tau) \qquad (4)$$

with τ = 54 s. Also shown in the figure is a set of data depicting how *f* decreased for a PSf-*g*-PAA membrane with time after pH = 8.0 water was introduced for permeability testing. In this case, the *f* relaxation time τ was 20 s.

Size Selectivity. To estimate the size of the constricting pores of the membranes, we performed a PEG permeation test. In this experiment, a PSf-*g*-PAA_{90} membrane was used to compartment two half-cells. Two PEG samples with M_w = 3070 and 960 g/mol were placed in one-half cell. Our SEC study showed that only the PEG sample with M_w = 960 g/mol or PEG-960 permeated the membrane but not the sample with M_w = 3070 g/mol after 24 h. Assuming an average statistical bond length of 0.5 nm and Gaussian chain statistics for the PEG samples in water, we estimated the radii of gyration of 1.7 and 3.0 nm for the lower and higher molar mass sample, respectively. Thus, the size of the constricting pores in this membrane should be between 1.7 and 3.0 nm.

A more quantitative permeation kinetic analysis was performed for the PEG-960 sample with data shown in Figure 8. The data seem to follow the trend typical of gas permeation across dense membranes. In both instances a period of time elapsed before PEG-960 broke

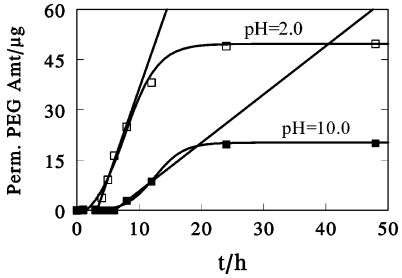

Figure 8. Increase in permeated PEG-960 amount through a PSf-*g*-PAA_{90} membrane as a function of time at pH = 2.0 (□) and pH = 10.0 (■), respectively.

through the membrane. Figure 8 also shows the extrapolation of data to the *t* axis in the region where the permeated amount increased linearly with time. At pH = 2.0 and pH = 10.0, these times are 3.23 and 6.06 h, respectively. Since our membranes are asymmetric and the thickness of the rate-limiting skin layer is unknown, these data were not used to calculate the diffusion coefficients of PEG-960 in the membranes. The data nonetheless show that PEG-960 permeated more slowly at pH = 10.0 due to the increased blocking of the pores by the more extended PSA chains.

To estimate the maximum amount of PEG-960 that could have permeated the membrane, we made use of the fact that the initial PEG-960 solution concentration and volume on the feed side were 10.0 ppm and 13.00 mL, respectively. Subsequently, nine samples at a total volume of 2.00 mL were taken out from the permeate side, and the sample taking was accompanied by the removal of an equal amount of liquid from the feed side. At a final volume of 11.00 mL for the feed, the maximum of PEG-960 that could have passed the membrane would have been ~55 μg provided that the membrane had not separated the sample based on molar mass. In reality, the amount of PEG-960 permeated after 2 days was ~50 μg at pH = 2.0 and ~20 μg at pH = 10.0. The incomplete permeation of PEG-960 at pH = 10.0 again suggests the more pronounced blocking of the pores by the PSA chains.

Additional experiments conducted in our laboratory demonstrated that PEG-960 did not penetrate the PSf-*g*-PAA_{340} membranes. This is most probably due to the long PAA chains blocking the pores more efficiently. This more efficient pore blocking has been seen in Figure 5 to lead to lower water fluxes for these membranes. The more surprising result was that PEG-960 did not permeate the PSf-*g*-P*t*BA_{90} membranes either despite the fact they had a slightly higher water flux than the PSf-*g*-PAA_{90} membranes. While we do not have a definitive explanation for this phenomenon, we believe this may be related to the incompatibility between the PEG and the P*t*BA chains.

Salt Permeation Data. Figure 9 shows the salt permeation data of a PSf-*g*-PSA_{90} membrane. Data of similar trends were seen for the PSf-*g*-PAA_{90} and PSf-*g*-PSA_{340} membranes. NaCl and $BaCl_2$ evidently permeated the membranes much faster than Na_2SO_4 and $K_3Fe(CN)_6$, and the permeated amount m_t increased with *t* for the former two salts following

$$m_t = m_\infty(1 - \exp(-t/\tau)) \qquad (5)$$

where m_∞ is the permeated amount at infinite times. Table 4 summarizes the τ and m_∞ values obtained from fitting the experimental NaCl and $BaCl_2$ data using eq

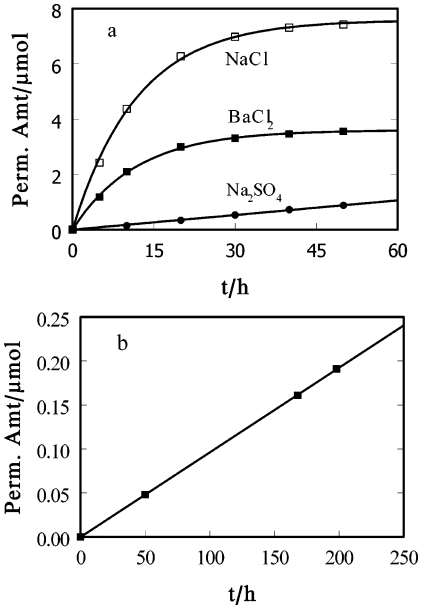

Figure 9. (a) Variation in the amount of NaCl (□), $BaCl_2$ (■), and Na_2SO_4 (●) permeated through a PSf-*g*-PSA_{90} membrane as a function of time. Part b shows how the amount of $K_3[Fe(CN)_6]$ (■) permeated changed as a function of time.

Table 4. Values of m_∞ and τ for the Transport of Different Salts across PSf-*g*-PAA and PSf-*g*-PSA Membranes

feed solution	τ/h	m_∞/μmol	m_∞/m_{th}
PSf-*g*-PAA_{90} Membrane			
NaCl (1.00×10^{-3} M)	11.1	7.6	1.01
$BaCl_2$ (0.50×10^{-3} M)	12.1	3.6	0.96
Na_2SO_4 (0.50×10^{-3} M)	260	3.8[a]	
PSf-*g*-PSA_{90} Membrane			
NaCl (1.00×10^{-3} M)	27.5	7.9	1.04
$BaCl_2$ (0.50×10^{-3} M)	23.7	3.8	1.02
Na_2SO_4 (0.50×10^{-3} M)	334	3.8[a]	
$K_3[Fe(CN)_6]$ (0.33×10^{-3} M)	2600	2.5[a]	
PSf-*g*-PSA_{340} Membrane			
NaCl (1.00×10^{-3} M)	11.9	7.6	1.00
$BaCl_2$ (0.50×10^{-3} M)	11.7	3.6	0.95
Na_2SO_4 (0.50×10^{-3} M)	207	3.8[a]	

[a] These are the theoretical m_∞ values.

5. In the last column, m_∞ is compared with the theoretical maximal permeated amount m_{th}, and all of the m_∞/m_{th} values are close to 1 for NaCl and $BaCl_2$ transport. This suggests the eventual uniform partition of the salts between the two half-cells.

Because of the slow transport of Na_2SO_4 and $K_3Fe(CN)_6$, it was impractical to follow the whole permeation process of these salts. To obtain τ for the transport of these salts, we assumed the validity of eq 5. At short times, we approximated the exponential term by $(1 - t/\tau)$, and eq 5 was thus reduced to

$$m_t = m_\infty(t/\tau) \qquad (6)$$

The τ values were obtained from the slope of the m_t vs *t* line by using eq 6 and plugging in m_{th} for m_∞.

In summary, results of Table 4 allude to the following trends. First, the permeation rate as characterized by τ barely changed for a given membrane by changing NaCl to $BaCl_2$. This suggests that the cation valence change had a minimal effect on salt permeation rate. Second, τ increased as the salt changed from NaCl to Na_2SO_4 and then to $K_3Fe(CN)_6$. Thus, increasing the valence of the anions decreased the salt transport rate

drastically. Third, the transport rate of a given salt decreased as the membrane was changed from PSf-*g*-PAA_{90} to PSf-*g*-PSA_{90}.

Effect of Ion Valence Change. In the absence of an electric potential drop, the ion flux of a particular species across a membrane is given by[9a]

$$J = -D\frac{c_h^M - c_l^M}{l} \tag{7}$$

where c_h^M and c_l^M denote the concentrations of the species in the surface layers of the membrane on the higher and lower concentration sides, respectively; D is the diffusion coefficient of the species; and l is the thickness of the membrane. Assuming that c_h^M and c_l^M are related to the concentrations c_h and c_l of the species in the solution phase by $r_h c_h$ and $r_l c_l$ and considering the flux only at short times when $c_l \to 0$, we have

$$J = -Dr_h\frac{c_h}{l} \tag{8}$$

Since the transporting pores in our membranes are much larger than the size of the ions, the diffusion coefficients should be approximately the same as those in water for the ions. For Na^+, K^+, Ba^{2+}, Cl^-, and $Fe[(CN)_6]^{3-}$ in water at 25 °C, the diffusion coefficients are 1.33×10^{-5}, 1.95×10^{-5}, 0.847×10^{-5}, 2.03×10^{-5}, and 0.896×10^{-5} cm^2/s, respectively.[10] These values differ over a very narrow range, and the variation cannot explain the drastic difference in the transport rate of the four salts discussed here. The large τ variation range has to be explained mostly by the r_h change of the ions in the membranes.

As mentioned before, we expect the membranes to reject anions because they contain the negatively charged immobile PAA chains and a Donnan potential exists between the membranes and the surrounding aqueous solution.[1] For a membrane containing immobile anions in equilibrium with an aqueous solution of a salt that dissociates according to

$$M_vX_u \to vM^{k+} + uX^{l-} \tag{9}$$

expressions have been derived for the concentrations of the various mobile ions in the membrane phase and the aqueous solution.[9b] If we assume that the concentrations of the ions in solution are low as in our case so that their activity coefficients approach 1 and also the concentration of the fixed anions c_{R^-} inside the membrane is much higher than that of their co-ions X^{l-}, the following relation holds:

$$r_- = c_-^M/c_-^s = \left(\frac{lc^s}{c_{R^-}}\right) \tag{10}$$

where c^M and c^s denote X^{l-} concentrations in the membrane and aqueous phases, respectively. For the counterions M^{k+}

$$r_+ = c_+^M/c_+^s = \frac{c_{R^-}}{lc^s} \tag{11}$$

As mentioned before, $lc^s/c_{R^-} \ll 1$ in our case. Equations 10 and 11 suggest that the concentration of the co-ions X^{l-} decreases and that of the counterions M^{k+} increases inside a membrane relative to the aqueous phase. Since the counterions and co-ions have to transport simultaneously to maintain electric neutrality, the transport of the co-ions is rate-limiting. This explains why NaCl and $BaCl_2$ had a similar transport rate. For the salts NaCl, Na_2SO_4, and $K_3Fe[(CN)_6]$, we measured permeability at the constant value of $lc^s = 1.00 \times 10^{-3}$ M. While k was constant at 1 for the three salts, the l value increased from 1 to 2 and 3. Equations 8 and 10 suggest that the square and cubic power of the rate of NaCl transport should be approximately those of Na_2SO_4 and $K_3Fe[(CN)_6]$ transport. These are indeed in agreement with the τ values obtained.

Salt Transport Rates of the PSf-*g*-PAA_{90} and PSf-*g*-PSA_{90} Membranes. Since the permeation of the PSf-*g*-PAA and PSf-*g*-PSA membranes was measured using salt solutions prepared from distilled water, the exact pH and thus the degree of acrylic acid group dissociation were unknown. Despite this, the degree of acrylic acid group dissociation and thus c_{R^-} should be higher in the PSf-*g*-PSA than in the PSf-*g*-PAA membrane. An increase in c_{R^-} should, according to eq 10, reduce co-ion concentration in the membrane and therefore decrease salt transportation rate in agreement with the τ value variation trend seen in Table 4. An increase in c_{R^-} also helps expand the PAA chains and slow down water permeation. Because of this, the slower permeation of salts across the PSf-*g*-PSA membrane may have complex causes.

IV. Conclusions

PSf-*g*-P*t*BA membranes have been prepared from immersion into water of solution films of the polymers in MP/PA. The membranes, as confirmed by SEM and TEM studies, possessed asymmetric structures. The polymer in the skin layer formed a nodular phase consisting of fused polymer lumps. Surrounding the lumps were void channels. PSf-*g*-PAA membranes were obtained after the hydrolysis of P*t*BA in the PSf-*g*-P*t*BA membranes. The hydrolysis seemed to have led to the collapse of the larger cavities in the original PSf-*g*-P*t*BA membranes but not the smaller pores. PAA chains seemed to concentrate at the lump/lump or lump/pore interfaces. Both the PSf-*g*-P*t*BA and PSf-*g*-PAA membranes had high water permeability. The water permeability of the PSf-*g*-PAA membranes could be tuned by changing the permeant pH or ionic strength. The size of the constricting pores in the PSf-*g*-PAA_{90} membranes at pH = 2.0 should be ~2 nm as established by a PEG permeation experiment. The pore size decreased at pH = 10.0. Because of the immobile negative charges of the PAA, such membranes separated anions of different valences efficiently. The permeation data variation trend of different salts has been rationalized semiquantitatively.

Acknowledgment. Defence Research Development Canada and NSERC of Canada are gratefully acknowledged for sponsoring this research.

References and Notes

(1) See, for example: Mulder, M. *Basic Principles of Membrane Technology*, 2nd ed.; Kluwer Academic Publishers: Dordrecht, The Netherlands, 1996.
(2) See, for example: (a) Osada, Y.; Honda, K.; Ohta, M. *J. Membr. Sci.* **1986**, *21*, 327. (b) Mika, A. M.; Childs, R. F.;

Dickson, J. M.; McCarry, B. E.; Gagnon, D. R. *J. Membr. Sci.* **1995**, *108*, 37. (c) Ito, T.; Hioki, T.; Yamaguchi, T.; Shinbo, T.; Nakao, S.; Kimura, S. *J. Am. Chem. Soc.* **2002**, *124*, 7840. (d) Liang, L.; Shi, M. K.; Viswanathan, V. V.; Peurrung, L. M.; Young, J. S. *J. Membr. Sci.* **2000**, *177*, 97.

(3) See, for example: (a) Zhai, G. Q.; Toh, S. C.; Tan, W. L.; Kang, E. T.; Neoh, K. G.; Huang, C. C.; Liaw, D. J. *Langmuir* **2003**, *19*, 7030. (b) Ying, L.; Wang, P.; Kang, E. T.; Neoh, K. G. *Macromolecules* **2002**, *35*, 673. (c) Ying, L.; Kang, E. T.; Neoh, K. G. *J. Membr. Sci.* **2002**, *208*, 361. (d) Ying, L.; Kang, E. T.; Neoh, K. G. *Langmuir* **2002**, *18*, 6416. (e) Park, E.-S.; Yoon, J. S. *J. Appl. Polym. Sci.* **2001**, *82*, 1658.

(4) Lu, Z. H.; Liu, G. J.; Duncan, S. *Macromolecules* **2004**, *37*, 174.

(5) For a review on membranes of PSf derivatives, see, for example: Guiver, M. D.; Robertson, G. P.; Yoshikawa, M.; Tam, C. M. In *Membrane Formation and Modification*; Pinnau, I., Freeman, B. D., Eds.; ACS Symposium Series 744; American Chemical Society: Washington, DC, 2000.

(6) Han, M. J. *Desalination* **1999**, *121*, 31.

(7) (a) Liu, G. J.; Ding, J. F.; Hashimoto, T.; Kimishima, K.; Winnik, F. M.; Nigam, S. *Chem. Mater.* **1999**, *11*, 2233. (b) Liu, G. J.; Ding, J. F. *Adv. Mater.* **1998**, *10*, 69. (c) Liu, G. J.; Ding, J. F.; Guo, A.; Herfort, M.; Bazett-Jones, D. *Macromolecules* **1997**, *30*, 1851.

(8) Mark, H. F.; Bikales, N. M.; Overberger, C. G.; Menges, G.; Kroschwitz, J. I. *Encyclopedia of Polymer Science and Engineering*, 3rd ed.; John Wiley & Sons: New York, 1985; Vol. 1, p 228.

(9) See, for example: Lakshminarayanaiah, N. *Transport Phenomena in Membranes*; Academic Press: New York, 1969; (a) p 95 and (b) p 89.

(10) See, for example: Lide, D. R.; Frederikse, H. P. R. *CRC Handbook of Chemistry and Physics*, 76th ed.; CRC Press: Boca Raton, FL, 1995.

MA049954Q